Design and Analysis of Sliding Window ARQ Protocols with Rate Adaptation for Burst Transmission over FSO Turbulence Channels

Hoang D. Le, *Student Member, IEEE,* Vuong V. Mai, *Member, IEEE,* Chuyen T. Nguyen, and Anh T. Pham, *Senior Member, IEEE*

***Abstract*—This paper studies a cross-layer design of error-control protocols with rate adaptation for free-space optical (FSO) burst transmission over atmospheric turbulence channels. Specifically, sliding window automatic repeat request (ARQ) protocols are designed so that the window size is determined by the burst duration. This facilitates an effective operation of sliding window protocols with the adaptive rate (AR) transmission over the atmospheric turbulence channels. To analyze the performance of the design, the time-varying behavior of the atmospheric turbulence channels, modeled by the popular Gamma-Gamma (ΓΓ) distribution, is captured to develop the burst error model. An embedded Markov model, which is formulated in the discrete time defined by burst duration, is analyzed based on the developed burst error model. Using the queueing analysis, the frame loss rate, average delay, and system throughput are analytically derived. Numerical results quantitatively demonstrate the impact of atmospheric turbulence on the system performance and support the optimal selection of system parameters over turbulence conditions. Monte Carlo simulations are also performed to validate the analytical results, and an excellent agreement between the analytical and simulation results is confirmed.**

***Index Terms*—Free space optical (FSO) systems, atmospheric turbulence, automatic repeat request (ARQ), sliding window protocols, adaptive rate (AR) transmission, cross-layer design, Markov chain.**

I. Introduction

THE growing demand of high data rate transmission has become the main challenge for the design of the next generation of wireless communication networks [1]. To meet this requirement, free-space optical (FSO) communication is being considered as a promising complementary solution to the current radio frequency (RF) in the wireless backhaul networks [2], [3]. While the FSO communication offers many advantages, e.g., license free, huge bandwidth, ease of deployment, high security and low installation cost, the uncertainty of the atmospheric links, especially the signal fading due to the atmospheric turbulence poses various challenges in the system design [4], [5].

Over the past decade, there have been many studies on error-control focusing on the FSO physical (PHY) layer performance enhancement over turbulence-induced fading channels [6]–[12]. In the link layer, automatic repeat request (ARQ) is the most popular error-control protocol. ARQ can be classified into two types: stop-and-wait (SW) and sliding window protocols; and both of them have been intensively studied in wired and wireless systems. In the domain of FSO, however, there has been only several studies on the performance of SW-ARQ over turbulence-induced fading channels thanks to its simplicity in analysis [13]–[16]. Particularly, Kiasaleh *et al*. analyzed and compared the frame error rate of SW-ARQ and hybrid-ARQ (H-ARQ) protocols for a weak turbulence scenario in [13]. The performance of SW-ARQ combined with error-correcting code in terms of outage probability and throughput over weak-to-strong turbulences was investigated in [14]. In [15], authors considered the delay issue of ARQ under impacts of different channel state information (CSI) over FSO fading channels. Most recently, an integration of SW-ARQ and adaptive rate (AR) transmission to improve the system performance over atmospheric turbulence channels was presented in [16].

SW-ARQ is, however, not practically useful, especially in point-to-point high-speed systems, due to its inefficient bandwidth utilization. Practical systems employ the sliding window protocols, which allows higher efficiency thanks to the fact that many frames can be continuously transmitted without waiting for the acknowledgement. In the design and analysis of the sliding window protocols in FSO systems, one of the key issues could come from the modeling of the time-varying behavior of turbulence-induced fading channels. For FSO links operating at high data rates, since the temporal correlation time of the atmospheric turbulence process is the order of tens of milliseconds (i.e. the slow fading), the loss probabilities of frames are highly correlated, i.e., frame errors tend to occur in bursts [17], [18]. In previous studies, the time-varying behavior of atmospheric turbulence and the burst error issues were not considered as SW-ARQ only transmits single frame per round trip time. Due to the transmission of multiple frames, addressing these issues in sliding window ARQ is critical, yet not well investigated.

The initial study on the sliding window ARQ protocols has been recently reported [19], [20], in which only throughput performance was modeled and analyzed. In addition, these studies assumed that the transmitter queue is infinite and always loads the frames for transmission. For practical design with finite queue size and random traffic, the statistical behavior of the arrival process and the finite-size queueing model

This work was presented in part at CSNDSP 2018 and ICTC 2018.

Hoang D. Le and Anh T. Pham are with the Computer Communications Lab., The University of Aizu, Aizuwakamatsu 965-8580, Japan.

Vuong V. Mai is with Photonics Systems Research Laboratory, KAIST, Korea, and Chuyen T. Nguyen is with the School of Electronics and Telecommunications, Hanoi University of Science and Technology, Vietnam

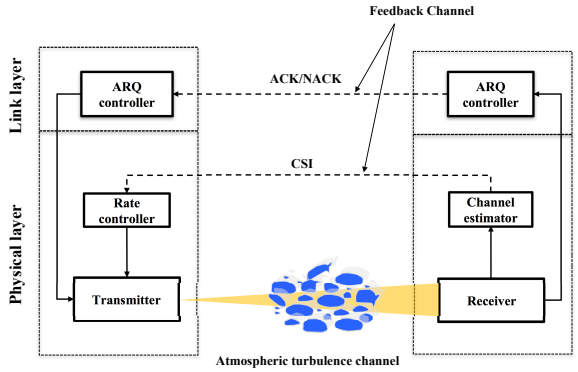

Figure 1: FSO system using sliding window ARQ and AR.

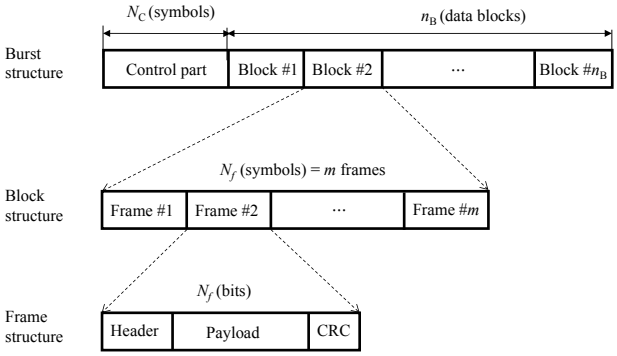

Figure 2: The data unit structure.

need to be taken into account. The performance of FSO relay systems using stop-and-wait mechanism with finite queues has been analyzed in [21], [22]. To the best of our knowledge, the performance of sliding ARQ with queueing model has been only investigated in the domain of RF communications [23]–[25]. As the fading channel models in FSO are completely different from that of RF, it would be crucial to have the proper protocol design under the atmospheric turbulence conditions for the optimization of FSO system performance.

In this paper, we present a comprehensive cross-layer design and an insightful analysis based on queueing theory. Both sliding window protocols, namely go-back-n (GBN) and selective repeat (SR) are considered. Also, their integration with AR transmission is considered to further improve the system performance. To effectively facilitate the operation of sliding window protocols with the AR transmission over the turbulence channels, the window size, which is based on the burst duration, is designed considering the time-varying behavior of the turbulence-induced fading channels. The weak-to-strong atmospheric turbulence is modeled by Gamma-Gamma ($\Gamma\Gamma$) distribution, and the time-varying behavior of the turbulence channel is modeled by a finite Markov chain. The channel model is then used to develop the burst error model. A queueing model is analyzed based on a Markov model developed from burst error model for the cross-layer performance analysis. Numerical results quantify the impacts of atmospheric turbulence on the system performance metrics including frame error rate, average delay, and throughput, and discuss the optimal selection of system parameters.

The remainder of the paper is organized as follows. The system description is presented in Section II. The channel model analysis and burst error model are shown in Section III. The queueing model for the cross-layer performance analysis is investigated in Section IV. Numerical results are given in Section V. Finally, Section VI concludes the paper.

II. System Description

Figure 1 describes the considered FSO system using the link-layer sliding window protocol, which can be either GBN-ARQ or SR-ARQ, and adaptive rate (AR) transmission at PHY layer over turbulence fading channels. The AR transmission aims to maximize the data rate over the fading channels while satisfying a pre-defined Quality of Service (QoS), i.e., a

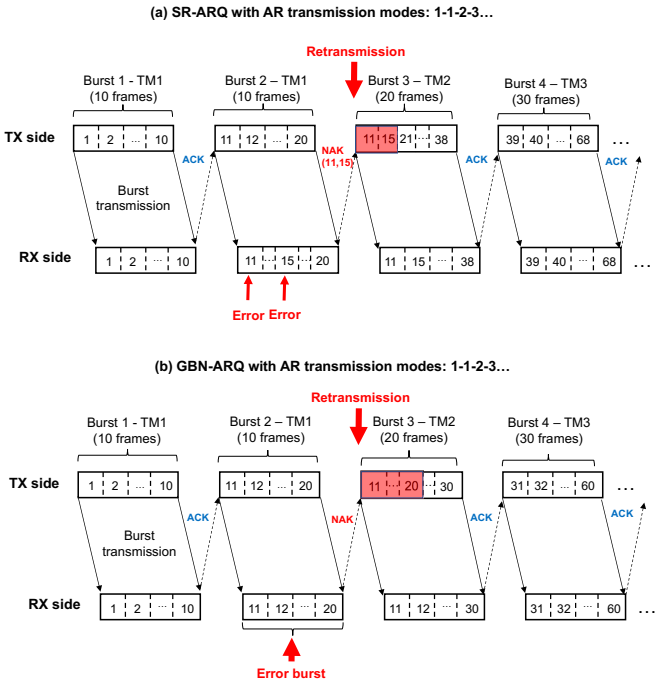

Figure 3: An example of the operation of (a) SR-ARQ and (b) GBN-ARQ protocols with AR transmission; window size = 1 burst time.

targeted frame-error rate (denoted as $\text{FER}_{\text{target}}$). We adopt the subcarrier M-ary quadrature amplitude modulation (M-QAM) schemes as in [26], [27] with a fixed symbol rate of R_s for the L possible transmission modes. The similar receiver noise model and $\Gamma\Gamma$ channel model for atmospheric turbulence as in [26] are assumed. The transmission bit rate and information rate, change for every mode and are given as $R_b = R_s \log_2(M)$ (bits/sec) and $m = \log_2(M)$ (bits/symbol), respectively, where M is the constellation size. Let $\gamma_1^* < \gamma_2^* < \cdots < \gamma_L^*$ be the switching thresholds for different transmission modes, and γ be the instantaneous signal-to-noise ratio (SNR), i.e., the channel state information (CSI). The transmission mode n is selected if $\gamma_n^* \le \gamma < \gamma_{n+1}^*$, where $n \in \{1, 2, \cdots, L-1\}$ and to avoid a high frame error rate, no transmission is allowed when $\gamma < \gamma_1^*$. These thresholds can be obtained by a least-square curve fitting of the frame error rate (FER) [28].

At the PHY layer, data is transmitted in fixed-time bursts

whose the time duration is chosen to be shorter than the fading channel coherence time. Each burst consists of (1) a control part with N_C symbols modulated by SC-BPSK scheme (so that the receiver can always demodulate this part), and (2) a data part with n_B data blocks; each block has exactly N_f symbols, which can be adaptively modulated by M-QAM schemes depending on the CSI feedback from the receiver[1], i.e. each block consists of exactly $m \times N_f$ data bits. Given the size of link-layer data frame of N_f bits, there are m frames per block, or in other words, $n_B \times m$ frames per burst. The burst/block and frame structures are illustrated as in Fig. 2.

The ARQ protocol operates at the link layer to detect and retransmit corrupted frames. To detect frame error, the standard cyclic redundancy check (CRC) scheme is used, and for the sake of simplicity, we assume that frame error is always detectable by the CRC. The operation of both GBN-ARQ and SR-ARQ is applied to each data burst consisting of multiple frames. The transmissions occur in the fixed-size time slots, which are equal to the burst durations. Feedback signal (either ACK or NACK), which is also assumed to be error-free, is returned by the receiver in unit of a data burst transmission, which aims to reduce the network traffic over high-speed channels. In case of transmission failure, all the frames in whole window size defined as N time slots will always be re-transmitted in GBN-ARQ, while SR-ARQ only retransmits the erroneous frames based on a NAK message from receiver that indicates the sequence numbers of those frames.

Example: The operation of SR-ARQ and GBN-ARQ is illustrated in Fig. 3, where the window size is set to $N = 1$ burst time, $n_B = 10$ blocks/burst. In Fig. 3(a), the frames 11 and 15 in burst 2 are assumed to be in error, and when a NAK message, which indicates the sequence numbers of erroneous frames (11 and 15) arrives at the transmitter side, SR-ARQ protocol retransmits "selectively" these frames in burst 3, together with the new frames. For the GBN-ARQ protocol in Fig. 3(b), burst 2 is assumed to be in error when any of frame in this burst is erroneous. And when the NAK for burst 2 arrives at the transmitter side, all the frames from 11 to 20 in the window size are retransmitted even though some frames were correctly received before.

The link-level transmitter buffer (queue) for both GBN-ARQ and SR-ARQ protocols operates in a first-in-first-out (FIFO) mode and can store up to $\bar{Q}$ frames. Frames will be removed from the buffer after receiving ACK messages from receiver. The maximum number of retransmissions allowed for a frame is supposed to be unbounded. Therefore, the delay obtained in this paper can be considered as an upper bound for the case where a finite number of retransmissions is allowed at the link layer.

In summary, the assumptions used in this paper are described as below. 1) The channel time is partitioned into constant time intervals called slots. 2) Each data burst containing multiple frames, is transmitted in a time slot whose length is fixed-value of a burst duration. 3) An error-free feedback channel is available for carrying both CSI and ACK/NAK information. 4) The maximum number of ARQ retransmissions is assumed to be infinite. 5) The receiver buffer capacity is equal to the maximum number of frames that can be transmitted in a burst so that frame losses are not happend at the receiver side.

[1]Practically, this CSI estimation can be done at the transmitter due to the reciprocity in bidirectional FSO channels, which was verified in [29].

III. Channel Modeling and Burst Error Model

In our design, data is transmitted in fixed-time bursts. Thus, it is necessary to capture the time-varying behavior of turbulence fading channels to model the behavior of data burst error. To do so, we first review the turbulence fading channel model and its important characteristic of level-crossing rate (LCR). The channel-state is modeled to facilitate the operation of sliding window protocols with AR under impact of atmospheric turbulence. Then, a data burst error model is developed from the channel-state model due to the transmissions of multiple frames over turbulence fading channels.

A. Turbulence Fading Channel Model

The atmospheric turbulence phenomenon causes the scintillation effect, which results in signal fluctuations at the receiver. The $\Gamma\Gamma$ model is considered to be the most suitable for describing a wide range of turbulence conditions, from weak to strong. The probability density function (PDF) of received SNR, γ, is given as

$$f_\gamma(\gamma) = \frac{(\alpha\beta)^{\frac{\alpha+\beta}{2}}}{\Gamma(\alpha)\Gamma(\beta)\bar{\gamma}^{\frac{\alpha+\beta}{4}}} \gamma^{\frac{\alpha+\beta}{4}-1} K_{\alpha-\beta}\left(2\sqrt{\alpha\beta\sqrt{\frac{\gamma}{\bar{\gamma}}}}\right), \quad (1)$$

where $\bar{\gamma}$ is the average value of γ, $\Gamma(.)$ is the gamma function, and $K_{\alpha-\beta}(.)$ is the modified Bessel function of second kind of order $\alpha-\beta$ [30]. The parameters α and β, which are the effective numbers of large-scale and small-scale eddies of scattering environment, respectively, can be written as

$$\alpha = \left\{\exp\left[\frac{0.49\sigma_R^2}{\left(1+1.11\sigma_R^{12/5}\right)^{7/6}}\right]-1\right\}^{-1},$$
$$\beta = \left\{\exp\left[\frac{0.51\sigma_R^2}{\left(1+0.69\sigma_R^{12/5}\right)^{5/6}}\right]-1\right\}^{-1}. \quad (2)$$

Here, σ_R^2 is the Rytov variance, and in the case of plane wave propagation, it is given by

$$\sigma_R^2 = 1.23 C_n^2 k^{7/6} d^{11/6}, \quad (3)$$

where $k = 2\pi/\lambda$ is the optical wave number, in which λ is the optical wavelength, d is the channel distance, and C_n^2 is the altitude-dependent index of the refractive structure parameter, which varies from $10^{-17}\mathrm{m}^{-2/3}$ to $10^{-12}\mathrm{m}^{-2/3}$ [4]. Typically, weak, moderate, and strong turbulence conditions correspond to $\sigma_R^2 < 1$, $\sigma_R^2 \simeq 1$, and $\sigma_R^2 > 1$, respectively, while the saturation regime is defined by $\sigma_R^2 \to \infty$ [8]. Its cumulative distribution function (CDF) is also given as

$$F_\gamma(\gamma) = \frac{1}{\Gamma(\alpha)\Gamma(\beta)} G_{1,3}^{2,1}\left[\alpha\beta\sqrt{\frac{\gamma}{\bar{\gamma}}}\middle| \begin{matrix} 1 \\ \alpha,\beta,0 \end{matrix}\right], \quad (4)$$

where $G_{p,q}^{m,n}[.]$ is the Meijer's G-function [16].

B. Level Crossing Rate

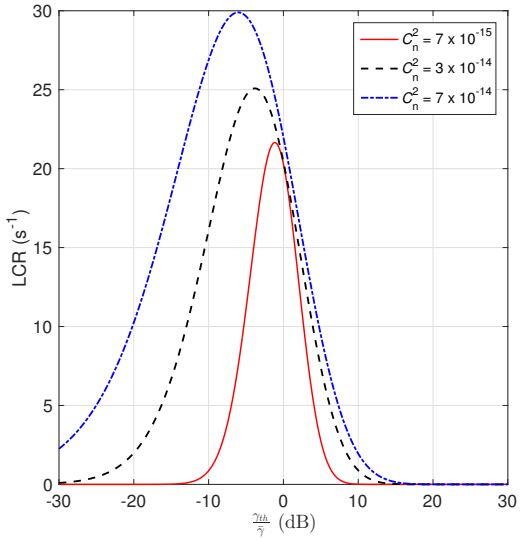

Figure 4: LCR vs. $\gamma_{\text{th}}/\overline{\gamma}$ with different turbulence strengths, given $\overline{\gamma} = 20$ dB, $d = 1000$ m, and $t_0 = 10$ ms.

The average LCR defined as the average number of times per second that the received SNR passes the certain threshold γ_{th} (either positive or negative direction), is given as

$$N(\gamma_{\text{th}}) = \frac{1}{2}\int_{-\infty}^{\infty} |\dot{\gamma}| f_{\gamma,\dot{\gamma}}(\gamma_{\text{th}}, \dot{\gamma}) d\dot{\gamma}, \tag{5}$$

where $\dot{\gamma}$ is the first derivative of γ with respect to time, $f_{\gamma,\dot{\gamma}}(\gamma_{\text{th}}, \dot{\gamma})$ is the joint PDF of $\gamma(t)$ and $\dot{\gamma}(t)$ at time t [31]. Based on the analysis in [32] and by inserting the relation between optical irradiance I and γ, i.e., $I = \sqrt{\gamma/\overline{\gamma}}$, the average LCR for ΓΓ fading model can be obtained as

$$N(\gamma_{\text{th}}) = \frac{\sqrt{\pi}\sigma_s \nu_0 \alpha^{\alpha}\beta^{\beta}}{\Gamma(\alpha)\Gamma(\beta)} \left(\sqrt{\frac{\gamma_{\text{th}}}{\overline{\gamma}}}\right)^{\beta-1/2} \int_0^{\infty} x^{\alpha-\beta-3/2} \sqrt{\sqrt{\frac{\gamma_{\text{th}}}{\overline{\gamma}}} + x^2} \times \exp\left[-\alpha x - \frac{\beta}{x}\sqrt{\frac{\gamma_{\text{th}}}{\overline{\gamma}}}\right] dx, \tag{6}$$

where σ_s^2 and ν_0 are the log-intensity variance and quasi-frequency, respectively. The log-intensity variance σ_s^2 that depends on the channel characteristics, is given as

$$\sigma_s^2 = \exp\left[\frac{0.49\sigma_{\text{R}}^2}{\left(1 + 0.18h^2 + 0.56\sigma_{\text{R}}^{12/5}\right)^{7/6}} + \frac{0.51\sigma_{\text{R}}^2}{\left(1 + 0.9h^2 + 0.62h^2\sigma_{\text{R}}^{5/6}\right)^{5/6}}\right] - 1, \tag{7}$$

here, $h = \sqrt{kD^2/4d}$, and D is the receiver aperture diameter [33]. In addition, the quasi-frequency, ν_0, defined as the number of times per second that $\gamma = \gamma_{\text{th}}$, can be written as

$$\nu_0 = \frac{1}{\sqrt{2}\pi t_0}, \tag{8}$$

where t_0 is the fading channel coherence time defined as the interval of time that the same scintillation coefficient is maintained [34]. Fig. 4 shows an example of LCR vs. $\gamma_{\text{th}}/\overline{\gamma}$ with different turbulence strengths. Obviously, LCR increases when the turbulence intensity becomes stronger.

C. Channel-State Model

We now design the channel-state model to effectively facilitate the operation of sliding window protocols with AR under impact of atmospheric turbulence. In particular, the data is transmitted in fixed-time bursts of $T_{\text{burst}} = (N_{\text{C}} + n_{\text{B}}N_f)/R_s$ in our sliding window ARQ design. Therefore, we first divide the channel into states defined by a range of SNR. The channel is said to be in state i-th if the received SNR falls into the interval of $[\gamma_i, \gamma_{i+1})$. The selection of the range of SNR satisfies the condition that the intervals of all channel-state, which are defined as the average duration that the received SNR a state, are equal; and these intervals are longer or equal to T_{burst}. The channel-state interval should also be shorter than the fading channel coherence time so that we can see the effect of correlated errors in each channel state.

The interval of channel-state i-th, $\overline{\tau}_i$, depends on the statistical characteristic of channel, and can be expressed as [35]

$$\overline{\tau}_i = \frac{\text{Pr}_i}{N(\gamma_i) + N(\gamma_{i+1})}, \tag{9}$$

where $N(\gamma_{\text{th}})$ is the level crossing rate at a certain threshold of γ_{th} and Pr_i is the probability of the channel state i-th, which is then expressed as

$$\text{Pr}_i = \int_{\gamma_i}^{\gamma_{i+1}} f_{\gamma}(\gamma) d\gamma = F_{\gamma}(\gamma_{i+1}) - F_{\gamma}(\gamma_i), \tag{10}$$

where $f_{\gamma}(\gamma)$ and $F_{\gamma}(\gamma)$ are the probability density function (PDF) and cumulative distribution function (CDF) of the channel SNR, as in Eqs. (1) and (4), respectively.

Now, we need to determine the threshold levels γ_i. It is important to note that these thresholds are not the same as γ_n^*, $n \in \{1, 2, ..., L\}$, which are used for the selection of transmission modes as discussed in Section II. To do so, we set the first channel-state $[\gamma_1, \gamma_2)$ to the outage, i.e. is equivalent to $\left[-\infty, \gamma_1^*\right)$ of the previous section and the $\overline{\tau}_i$ is set to T_{burst}. In this way, we can determine all threshold levels γ_i. The algorithm to search for the thresholds $\{\gamma_i\}_{i=1}^{K+1}$ can be summarized as follows

Step 1: Set $\gamma_1 = -\infty$, $\gamma_2 = \gamma_1^*$, and $i = 3$.

Step 2: For each i, search γ_i that satisfies

$$\overline{\tau}_i = T_{\text{burst}}, \tag{11}$$

with $\overline{\tau}_i$ is given in eq. 9.

Step 3: If $i < K + 1$, set $i = i + 1$, and go to step 2; otherwise, go to step 4.

Step 4: Set $\gamma_{K+1} = +\infty$.

After the above process, we can have $K + 1$ threshold levels corresponding to K channel states. A finite-state Markov channel (FSMC) model then can be used to model the behavior of the channel as illustrated in Fig. 5. Given the probability of

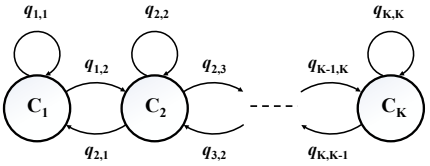

Figure 5: Channel-state transition model.

the channel-state i-th Pr_i, the transition probability from the state i-th to state j-th denoted by $q_{i,j}$ can be expressed by

$$q_{i,j} = \begin{cases} 0, & \text{if } |i-j| \geq 2 \\ \frac{N(\gamma_{i+1})T_{\text{burst}}}{\mathrm{Pr}_i}, & \text{if } j = i+1 \text{ and } i = 1,...,K-1 \\ \frac{N(\gamma_i)T_{\text{burst}}}{\mathrm{Pr}_i}, & \text{if } j = i-1 \text{ and } i = 2,...,K \\ 1 - q_{i,i+1} - q_{i,i-1}, & \text{if } i = j \text{ and } 0 < i < K \\ 1 - q_{0,1}, & \text{if } i = j = 0 \\ 1 - q_{K,K-1}. & \text{if } i = j = K \end{cases} \quad (12)$$

where $N(\gamma_{\text{th}})$ is given in eq. (6) and T_{burst} is the burst duration [16]. What remains now is to determine the transmission mode for each channel-state. In particular, each channel-state will be assigned a specific transmission mode, which can bring the highest possible data rate while maintaining a targeted $\mathrm{FER}_{\text{target}}$. The channel-state i-th with the SNR interval of $[\gamma_i, \gamma_{i+1})$, $i \in \{1,2,\cdots,N\}$, is said to be in transmission mode n if $\gamma_n^* \leq \gamma_{i+1} < \gamma_{n+1}^*$, where $n \in \{1,2,\cdots,L\}$ and the corresponding average FER satisfies $\mathrm{FER}_{\text{target}}$. If we denote by $\phi_i = \{n | i-\text{th state is assigned by mode } n\}$, the average frame error rate at state i-th using mode n, can be approximated by

$$\overline{\mathrm{FER}}_i = \int_{\gamma_i}^{\gamma_{i+1}} \mathrm{FER}(\gamma) f_\gamma(\gamma) d\gamma \simeq \int_{\gamma_i}^{\gamma_{i+1}} a_{\phi_i} \exp\left(-g_{\phi_i}\gamma\right) f_\gamma(\gamma) d\gamma, \quad (13)$$

where $\mathrm{FER}(\gamma)$ is the instantaneous FER, a_{ϕ_i} and g_{ϕ_i} are the curve fitting parameters given in Table I [28]. Note that the accuracy of the curve fitting approximation has been verified in [28], [36].

Table I: Example of Transmission Modes

	Mode 1	Mode 2	Mode 3	Mode 4
Modulation	BPSK	QPSK	8-QAM	16-QAM
m (bits/symbol)	1	2	3	4
a_n	48.1020	80.2966	99.8269	118.6961
g_n	1.0198	0.5058	0.1688	0.1013
γ_n^* (dB)	5.7959	9.3811	14.3584	16.7372

D. Burst Error Model

The burst error behavior can be modeled with good (G) and bad (B) states. In the adaptive-rate transmission, the good states consist of L sub-states corresponding to the L modes, i.e., G_n, $n \in \{1,2,\cdots,L\}$, as illustrated in Fig. 6.

In this structure, the system (in a specific transmission mode) is in a bad state when burst error happen, i.e. either the header or one of frames is corrupted with at least one bit error, while good states are those with error-free burst transmission. As it was assumed that frame errors are always detectable by the CRC, the burst-error probability at the channel-state i-th, denoted as BEP_i, can be given as

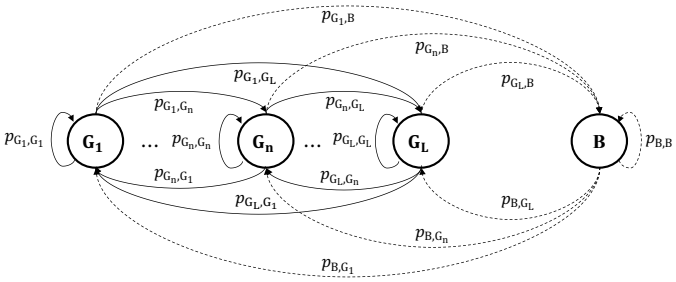

Figure 6: Burst error model.

$$\mathrm{BEP}_i = 1 - \left(1 - \overline{\mathrm{BER}}_{\mathrm{H},i}\right)^{N_{\mathrm{C}}} \times \left(1 - \overline{\mathrm{FER}}_i\right)^{n_{\mathrm{B}} \times m}, \quad (14)$$

where $\overline{\mathrm{FER}}_i$ is given in (13) and $\overline{\mathrm{BER}}_{\mathrm{H},i}$ is the average bit error rate for BPSK modulated control part of a burst at the channel state i-th [33].

The state transition probabilities of the mode-transmission process, which is shown in Fig. 6, are given by

$$\begin{aligned} p_{\mathrm{B,B}} &= \Pr\{\text{state B at } t+1 | \text{state B at } t\} \\ &= \frac{\Pr\{\text{state B at } t+1, \text{ state B at } t\}}{\Pr\{\text{state B at } t\}} \\ &= \frac{\sum_{i=1}^{K}\sum_{j=1}^{K} \mathrm{Pr}_i \mathrm{BEP}_i q_{i,j} \mathrm{BEP}_j}{\sum_{i=1}^{K} \mathrm{Pr}_i \mathrm{BEP}_i}, \end{aligned} \quad (15)$$

$$\begin{aligned} p_{\mathrm{B,G}_n} &= \Pr\{\text{state G}_n \text{ at } t+1 | \text{state B at } t\} \\ &= \frac{\sum_{i=1}^{K}\sum_{\phi_j=n} \mathrm{Pr}_i \mathrm{BEP}_i q_{i,j} \left(1 - \mathrm{BEP}_j\right)}{\sum_{i=1}^{K} \mathrm{Pr}_i \mathrm{BEP}_i}, \end{aligned} \quad (16)$$

$$\begin{aligned} p_{\mathrm{G}_n,\mathrm{B}} &= \Pr\{\text{state B at } t+1 | \text{state G}_n \text{ at } t\} \\ &= \frac{\sum_{\phi_i=n}\sum_{j=1}^{K} \mathrm{Pr}_i (1 - \mathrm{BEP}_i) q_{i,j} \mathrm{BEP}_j}{\sum_{\phi_i=n} \mathrm{Pr}_i (1 - \mathrm{BEP}_i)}, \end{aligned} \quad (17)$$

$$\begin{aligned} p_{\mathrm{G}_n,\mathrm{G}_l} &= \Pr\{\text{state G}_l \text{ at } t+1 | \text{state G}_n \text{ at } t\} \\ &= \frac{\sum_{\phi_i=n}\sum_{\phi_j=l} \mathrm{Pr}_i (1 - \mathrm{BEP}_i) q_{i,j} \left(1 - \mathrm{BEP}_j\right)}{\sum_{\phi_i=n} \mathrm{Pr}_i (1 - \mathrm{BEP}_i)}, \end{aligned} \quad (18)$$

where $n, l \in \{1,2,\cdots,L\}$, while $q_{i,j}$ and Pr_i are defined in the channel-state model. We can also re-write transition probabilities in a matrix form of $\mathbf{P}$ as (19).

On the other hand, we denote p_{B} and p_{G_n} be the steady-state probabilities of state B and state G_n, respectively, and $\mathbf{p} =$

$$\mathbf{P}=\left[\begin{array}{c|c}\mathbf{P}_{\mathrm{BB}} & \mathbf{P}_{\mathrm{BG}}\\ \hline \mathbf{P}_{\mathrm{GB}} & \mathbf{P}_{\mathrm{GG}}\end{array}\right]=\left[\begin{array}{c|cccccc} p_{\mathrm{BB}} & p_{\mathrm{BG}_1} & p_{\mathrm{BG}_2} & p_{\mathrm{BG}_3} & \cdots & p_{\mathrm{BG}_{L-1}} & p_{\mathrm{BG}_L}\\ \hline p_{\mathrm{G}_1\mathrm{B}} & p_{\mathrm{G}_1\mathrm{G}_1} & p_{\mathrm{G}_1\mathrm{G}_2} & p_{\mathrm{G}_1\mathrm{G}_3} & \cdots & p_{\mathrm{G}_1\mathrm{G}_{L-1}} & p_{\mathrm{G}_1\mathrm{G}_L}\\ p_{\mathrm{G}_2\mathrm{B}} & p_{\mathrm{G}_2\mathrm{G}_1} & p_{\mathrm{G}_2\mathrm{G}_2} & p_{\mathrm{G}_2\mathrm{G}_3} & \cdots & p_{\mathrm{G}_2\mathrm{G}_{L-1}} & p_{\mathrm{G}_2\mathrm{G}_L}\\ \vdots & \vdots & \vdots & \vdots & \ddots & \vdots & \vdots\\ p_{\mathrm{G}_{L-1}\mathrm{B}} & p_{\mathrm{G}_{L-1}\mathrm{G}_1} & p_{\mathrm{G}_{L-1}\mathrm{G}_2} & p_{\mathrm{G}_{L-1}\mathrm{G}_3} & \cdots & p_{\mathrm{G}_{L-1}\mathrm{G}_{L-1}} & p_{\mathrm{G}_{L-1}\mathrm{G}_L}\\ p_{\mathrm{G}_L\mathrm{B}} & p_{\mathrm{G}_L\mathrm{G}_1} & p_{\mathrm{G}_L\mathrm{G}_2} & p_{\mathrm{G}_L\mathrm{G}_3} & \cdots & p_{\mathrm{G}_L\mathrm{G}_{L-1}} & p_{\mathrm{G}_L\mathrm{G}_L}\end{array}\right]. \tag{19}$$

$\left[p_{\mathrm{B}}, p_{\mathrm{G}_1}, p_{\mathrm{G}_2}, \cdots, p_{\mathrm{G}_L}\right]$. According to the Markov chain theory, we have

$$\begin{cases}\mathbf{p}=\mathbf{p}.\mathbf{P},\\ p_{\mathrm{B}}+\sum_{n=1}^{L} p_{\mathrm{G}_n}=1.\end{cases} \tag{20}$$

By solving (20), we can finally obtain $\mathbf{p}$.

IV. Performance Analysis

This section focuses on the performance analysis of the sliding window ARQ protocols with AR transmission over atmospheric turbulence channels. In particular, we formulate a discrete time Markov model with time unit equals to one burst interval and the system states are observed at the beginning of each burst interval. We assume the Poisson frame arrival with rate ϑ (frames per burst time), the first-in-first-out (FIFO) policy and that frames arriving during burst time $t-1$ can only be transmitted in burst time t at the earliest. The queue size is finite and it can keep as many as Q frames; any arriving frame observing the queue full will be discarded.

The number of frames transmitted in a time slot for sliding window protocols is the minimum of the number of frames in the queue and the number of frames that can be transmitted depending on the AR modes. When a burst transmission, which contains multiple frames, is acknowledged, all the frames in that burst will be removed from the queue. If there is at least one erroneous received frame in a burst transmission, GBN-ARQ will retain all the transmitted frames in the queue, while SR-ARQ keeps erroneous ones for the retransmission and removes the successful ones from the queue. In order to analyze the queueing process induced by the sliding window ARQ and the AR transmission, we need to keep track not only the queueing states, which indicate the number of frames available in the queue at the observation point, but also the transmission states adopted from the burst error model in Section III. To do so, we newly develop a Markov model taking into account both queueing states and transmission states. Based on the developed model, the performance metrics including average frame loss rate, average frame delay, and average system throughput for both GBN-ARQ and SR-ARQ can be analytically derived.

A. Markov Model

Let $s(t)=(\xi_t,\rho_t)$ denote as the system state at a burst interval t, where $\xi_t\in\{0,1,\cdots,Q\}$ and $\rho_t\in\{\mathrm{B},\mathrm{G}_1,\cdots,\mathrm{G}_L\}$ represent the queueing state and the transmission state at this burst interval, respectively. The state $s(t)=(\xi_t,\rho_t)$ indicates that when the system is in transmission state ρ_t, there are ξ_t frames available in the queue at burst interval t. If we just look at the set of time instants $t=0,1,\cdots,\infty$, the transitions of $s(t)$ are Markovian. An embedded Markov model, as shown in Fig. 7, can be used to describe the protocol operation. The state space of this Markov model is $\mathbf{S}=\left\{S_\mu\right\}_{\mu=1}^{N_s}$, where $S_\mu=(\xi_\mu,\rho_\mu)$ and $N_s=(Q+1)(L+1)$. The transition matrix can be expressed as

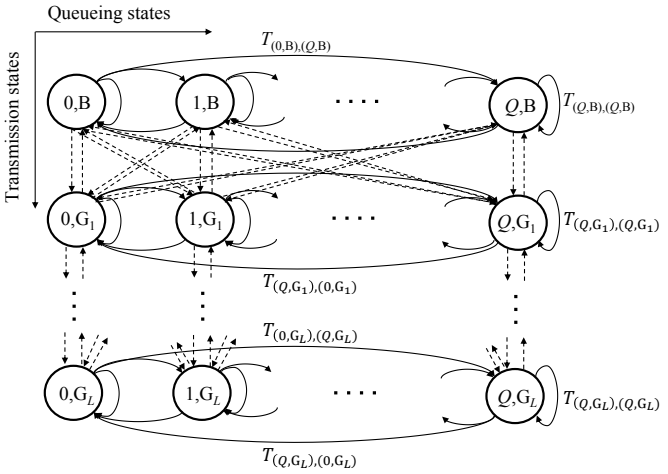

Figure 7: Markov model of the sliding window ARQ protocols with AR transmission.

$$\mathbf{T}=\begin{bmatrix}\mathbf{T}_{0,0} & \mathbf{T}_{0,1} & \cdots & \mathbf{T}_{0,Q}\\ \mathbf{T}_{1,0} & \mathbf{T}_{1,1} & \cdots & \mathbf{T}_{1,Q}\\ \vdots & \vdots & \ddots & \vdots\\ \mathbf{T}_{Q,0} & \mathbf{T}_{Q,1} & \cdots & \mathbf{T}_{Q,Q}\end{bmatrix}, \tag{21}$$

where the sub-matrix $\mathbf{T}_{u,v}$ is defined as

$$\mathbf{T}_{u,v}=\begin{bmatrix}T_{(u,\mathrm{B}),(v,\mathrm{B})} & T_{(u,\mathrm{B}),(v,\mathrm{G}_1)} & \cdots & T_{(u,\mathrm{B}),(v,\mathrm{G}_L)}\\ T_{(u,\mathrm{G}_1),(v,\mathrm{B})} & T_{(u,\mathrm{G}_1),(v,\mathrm{G}_1)} & \cdots & T_{(u,\mathrm{G}_1),(v,\mathrm{G}_L)}\\ \vdots & \vdots & \ddots & \vdots\\ T_{(u,\mathrm{G}_L),(v,\mathrm{B})} & T_{(u,\mathrm{G}_L),(v,\mathrm{G}_1)} & \cdots & T_{(u,\mathrm{G}_L),(v,\mathrm{G}_L)}\end{bmatrix}, \tag{22}$$

where $T_{(u,x),(v,y)}$ denotes by the transition probability from the state (u,x) to (v,y) with $u,v\in\{0,1,\cdots,Q\}$ and $x,y\in\{\mathrm{B},\mathrm{G}_1,\cdots,\mathrm{G}_L\}$ are queueing and transmission states, respectively. These transition probabilities can be computed as

$$\begin{aligned}T_{(u,x),(v,y)}&=\Pr(\xi_{t+1}=v,\rho_{t+1}=y|\xi_t=u,\rho_t=x)\\ &=\Pr(\xi_{t+1}=v|\xi_t=u,\rho_t=x)\times\Pr(\rho_{t+1}=y|\xi_t=u,\rho_t=x)\\ &=\Pr(\xi_{t+1}=v|\xi_t=u,\rho_t=x)\times\Pr(\rho_{t+1}=y|\rho_t=x),\end{aligned} \tag{23}$$

where $\Pr(\rho_{t+1}=y|\rho_t=x)$ denotes by the transition probability from transmission state x to y as given in (19). In addition,

$\Pr(\xi_{t+1}=v|\xi_t=u,\rho_t=x)$ is the probability that the number of frames in the buffer changes from u to v over one burst interval, given the transmission state at burst time t is x. It is obvious that when $v<Q$, this transition probability is equal to the probability that n_f frames are successfully acknowledged and removed from the buffer, given that there were u frames in the queue, and that the number of newly arrived frames is $v-(u-n_f)$, where $(n_f \le u)$.

When $v=Q$, we also need to consider the case where more frames arrive than the queue can accommodate, i.e., k frames arrive over one time slot with $k \ge Q-(u-n_f)$, this leads to a certain number of frame losses. Based on that, the transition probability $\Pr(\xi_{t+1}=v|\xi_t=u,\rho_t=x)$ for both GBN-ARQ and SR-ARQ can be commonly expressed as

$$\begin{aligned}&\Pr(\xi_{t+1}=v|\xi_t=u,\rho_t=x)=\\&=\begin{cases}P_A(v-(u-n_f))z_{n_f,u}, & \text{if } 0\le v<Q\\ \left(\sum_{k=Q-(u-n_f)}^{\infty}P_A(k)\right)z_{n_f,u}, & \text{if } v=Q\end{cases}\end{aligned} \tag{24}$$

where $z_{n_f,u}$ denotes the probability that n_f frames are removed from the queue, given that there were u frames in the queue, while $P_A(.)$ reflects the frame-arrival process. As the frame-arrival process during a time slot is assumed to be Poisson with intensity ϑ (in frames per time slot), the probability of having k frames arriving over a time slot is given by

$$P_A(k)=\begin{cases}\frac{\vartheta^k}{k!}\exp(-\vartheta), & \text{if } k\ge 0\\ 0. & \text{otherwise}\end{cases} \tag{25}$$

Besides, we separately determine the number of frames removed from the queue, n_f for GBN-ARQ and SR-ARQ. For the GBN-ARQ operation, all the frames transmitted during the current time slot will be retransmitted if the transmission state is in bad state. Otherwise, the number of frames transmitted during a time slot, given the transmission state of G_n, is equal to $\min\{n\times n_B,u\}$ (i.e., the actual number of frames transmitted during a particular time slot is the minimum of (i) the number frames available in the queue and (ii) the number of frames can be transmitted depending on the transmission state) with $n\times n_B$ corresponds to the number of frames transmitted in the transmission state G_n. Hence, the number of frames n_f of GBN-ARQ can be written as

$$n_{f_{\mathrm{GBN}}}=\begin{cases}\min\{n\times n_B,u\}, & \text{if } x=\mathrm{G}_n\\ 0. & \text{if } x=\mathrm{B}\end{cases} \tag{26}$$

For the SR-ARQ, the number of frames transmitted during a time slot, given the transmission state of G_n, is equal to $\min\{n\times n_B,u\}$, which is similar to GBN-ARQ. The difference between SR-ARQ and GBN-ARQ is in the reaction when the errors occur. The SR-ARQ only retransmits erroneous frames, while GBN-ARQ retransmits all the frames during a time slot. Therefore, the number of frames removed from the queue during a time slot n_f for SR-ARQ, given the system is in the bad state, can be written as

$$\begin{aligned}n_{f_{\mathrm{SR}}}=&\sum_{i=1}^{K}\Pr_i\sum_{j=1}^{\min\{\phi_i\times n_{\mathrm{B}}\}-1}j\binom{\min\{\phi_i\times n_{\mathrm{B}}\}-1}{j}(1-\overline{\mathrm{FER}}_i)^j\\&\times\overline{\mathrm{FER}}_i^{\min\{\phi_i\times n_{\mathrm{B}}\}-1-j}(1-\overline{\mathrm{BER}}_{\mathrm{H},i})^{N_C},\end{aligned} \tag{27}$$

where K is the number of channel states, $\Pr_i$ is the steady-state probability of the i-th channel-state, $\phi_i\times n_{\mathrm{B}}$ with $\phi_i=\{n|i-\text{th state is assigned by mode } n\}$ is the number of transmitted frames per burst corresponding to the i-th channel state, while FER_i is given in (13) and $\mathrm{BER}_{\mathrm{H},i}$ is the average bit error rate of header at the i-th channel state.

To complete our embedded Markov chain model, we now compute the probability $z_{n_f,u}$ for both GBN-ARQ and SR-ARQ, which can be commonly expressed as

$$z_{n_f,u}=\begin{cases}\begin{cases}p_{\mathrm{G}_n}, & \text{if } n_f=n\times n_{\mathrm{B}}\le u\\ \sum_{\phi_i=n}\pi_i(1-\overline{\mathrm{FER}}_i)^u, & \text{if } n_f=n\times n_{\mathrm{B}}>u\end{cases} & \text{if } x=\mathrm{G}_n\\ p_{\mathrm{B}}, & \text{if } x=\mathrm{B}\end{cases} \tag{28}$$

where p_{B} and p_{G_n} are the steady-state probability of state B and G_n, given in (20), respectively.

To derive the system performance measures, we need to obtain the stationary distribution of the Markov chain. In the equilibrium, a state $S_\mu=(\xi_\mu,\rho_\mu)$ has a probability of $\pi_{(\xi_\mu,\rho_\mu)}$. Let $\pi=[\pi_{(0,\mathrm{B})},\cdots,\pi_{(0,\mathrm{G}_L)},\cdots,\pi_{(Q,\mathrm{B})},\cdots,\pi_{(Q,\mathrm{G}_L)}]$ be the stationary distribution. Finally, we can obtain all elements of π by using standard Gaussian elimination to solve the following set of equations

$$\begin{cases}\pi\mathbf{T}=\pi,\\ \sum_{\xi_\mu=0}^{Q}\sum_{\rho_\mu=\mathrm{B}}^{\mathrm{G}_L}\pi_{(\xi_\mu,\rho_\mu)}=1,\end{cases} \tag{29}$$

where $\mathbf{T}$ is the transition matrix determined by (21).

B. Frame Loss Rate and Throughput

In our finite-queueing system, with the assumption of infinite persistence in the sliding window ARQ operation, the frames loss rate P_{loss} is simply equal to the queue overflow probability. To determine P_{loss}, we need to calculate the average frame losses over one burst interval. Let N_{loss} denote the average number of frame losses during a burst interval. Clearly, if more frames arrive than the queue can accommodate, they will be blocked and dropped. In particular, we assume that the queue contains u frames at the beginning of a burst interval and n_f frames are then successfully transmitted and removed from the queue during that interval, given that there are k frames arrive. As the queue only accommodate maximum Q frames, the number of frames that will be lost due to queue overflow can be calculated as, $\max\{0,k-[Q-(u-n_f)]\}$. So, the average number of frame losses N_{loss} can be computed by

$$N_{\mathrm{loss}}=\sum_{u=0}^{Q}\sum_{x=\mathrm{B}}^{\mathrm{G}_L}\pi_{(u,x)}z_{n_f,u}\sum_{k=Q-(u-n_f)}^{\infty}\{k-[Q-(u-n_f)]\}P_A(k), \tag{30}$$

where $z_{n_f,u}$ and $\pi_{(u,x)}$ are defined in (28) and (29), respectively, while $P_A(k)$ is the probability having k frames arrive the queue, as given in (25). The frame loss rate can then be determined as the ratio between the average number of frame losses due to the buffer overflow N_{loss} and the average number of arriving frames ϑ over one burst interval, i.e.,

$$P_{\text{loss}} = \frac{N_{\text{loss}}}{\vartheta}. \tag{31}$$

Then, given the frame loss rate P_{loss}, the system throughput for sliding window ARQ can be obtained by

$$\bar{\eta} = \vartheta(1 - P_{\text{loss}}). \tag{32}$$

where ϑ is the average arrival rate.

C. Average Frame Delay

The total average delay $\bar{D}$ (in number of burst intervals) for a frame in our system can be decomposed into two parts, namely 1) the average queueing delay, which is the time spent by a frame waiting in the queue and 2) the average service time which, is the time taken between removal of that frame from the link-layer queue for transmission and its error-free deliver to the higher layer at the receiver.

Let $\bar{D}_q$ denote the average queueing delay for a frame. Using Little's law, it can be calculated as

$$\bar{D}_q = \frac{N_q}{\vartheta(1 - P_{\text{loss}})}, \tag{33}$$

where N_q denote the average queue length, P_{loss} is the frame loss rate, and $\vartheta(1 - P_{\text{loss}})$ is the effective frame arrival rate [37]. With the stationary distribution $\mathbf{\Pi}$ computed in (29), we can calculate N_q as

$$N_q = \sum_{u=0}^{Q} \sum_{x=\text{B}}^{\text{G}_L} u \times \pi_{(u,x)}. \tag{34}$$

In addition to the queueing delay, let $\bar{D}_s$ denote the average service time for a frame. To calculate $\bar{D}_s$, we need to determine the average number of retransmissions of one frame, i.e.,

$$\bar{M} = \sum_{j=1}^{\infty} j p_{\text{retrans}}^{j-1}(1 - p_{\text{retrans}}) = \frac{1}{1 - p_{\text{retrans}}}, \tag{35}$$

where p_{retrans} is the probability of retransmission a frame. When the system is in bad state, a frame will always be retransmitted in GBN-ARQ despite error-free while SR-ARQ only retransmits that frame if it is in error. Therefore, the probability p_{retrans} can be expressed as

$$p_{\text{retrans}} = \begin{cases} p_{\text{B}}, & \text{for GBN-ARQ} \\ \sum_{i=1}^{K} \text{Pr}_i \overline{\text{FER}}_i, & \text{for SR-ARQ} \end{cases} \tag{36}$$

where K is the number of channel states, p_{B} is the probability of state B, Pr_i and $\overline{\text{FER}}_i$ are the probability and average frame error rate of the channel state i-th, respectively. So, the average service time can be calculated as

$$\bar{D}_s = (\bar{M} + 1)\frac{t_{\text{trans}} + t_{\text{prop}}}{T_{\text{burst}}}, \tag{37}$$

Table II: System Parameters

Name	Symbol	Value
Frame size	N_f	1500 bytes
Burst-control part size	N_{C}	40 symbols
Number of blocks/burst	n_{B}	30 blocks/burst
Burst time	T_{burst}	0.9 ms
Symbol rate	R_s	400 Msps
Coherence time	t_0	10 ms
Channel distance	d	1800 m
Receiver aperture diameter	D	0.02 m
Optical wavelength	λ	1.55 μm

where T_{burst} is the burst time, $t_{\text{trans}} = N_f/R_b$ is the frame transmission delay, where N_f and R_b are the frame size and bit rate, respectively. $t_{\text{prop}} = L/c$ is the frame propagation delay, where L and $c(= 3 \times 10^8$ m/s) are the channel distance and light speed, respectively. Finally, the average frame delay in our system can be evaluated as

$$\bar{D} = \bar{D}_q + \bar{D}_s, \tag{38}$$

where $\bar{D}_q$ and $\bar{D}_s$ are given by (33) and (37), respectively.

V. Numerical Results

This section presents and discusses the performance analysis of the proposed design with different parameter settings. Different turbulence strengths, i.e., $C_n^2 = 7 \times 10^{-15}\text{m}^{-2/3}$, $C_n^2 = 2 \times 10^{-14}\text{m}^{-2/3}$, and $C_n^2 = 10^{-13}\text{m}^{-2/3}$ for weak, moderate and strong turbulences, are considered. The parameters related to transmission modes are presented in Table I, and the other system parameters are given in Table II. Monte Carlo simulations are performed to validate the analytical results. In each burst time, the channel states are randomly generated according to the channel-state transition probabilities calculated in (12). For a given target frame error rate $\text{FER}_{\text{target}}$, a transmission mode is assigned in a specific channel state, which determines the maximum number of frames that can be transmitted. The number of frames successfully leaving the queue is determined based on the transmission states with corresponding probabilities from the Markov error model. The queue length is updated at every burst time by considering the frame arrivals, which follow the Poisson process with average arrival rate of ϑ (frames/burst time) and the number of successfully transmitted frames.

First, Fig. 8 quantitively highlights the benefits of sliding window protocols, both GBN and SR-ARQ, by comparing their throughputs with that of SW-ARQ under different symbol rates when $\text{FER}_{\text{target}} = 10^{-3}$, $Q = 150$ frames, $\vartheta = 90$ (frames/burst time) and $C_n^2 = 2 \times 10^{-14}\text{m}^{-2/3}$. First, we can verify a good agreement between analytical and simulation results, which confirm the correctness of the model and analysis. It is obvious that the sliding window protocols outperform the SW-ARQ due to transmitting of many fames without waiting the acknowledgement. The important point is that the throughput improvement becomes much more significant when the symbol rates are high, and this is exactly what we need from the FSO systems. This phenomenon is due to the fact that the time waiting for the acknowledgement of a data frame (two times of propagation delay) in SW-ARQ becomes significant

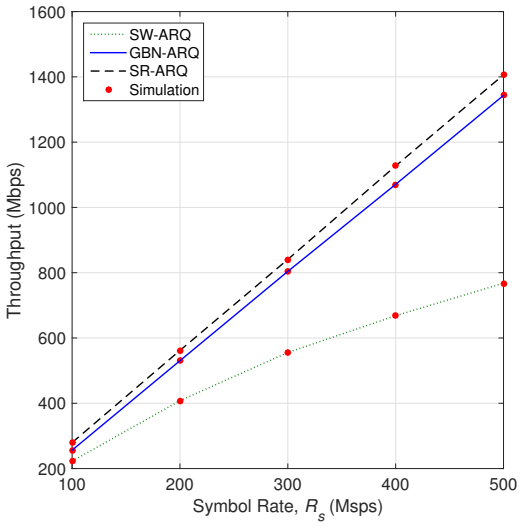

Figure 8: Sliding window and SW-ARQ throughput vs. symbol rates.

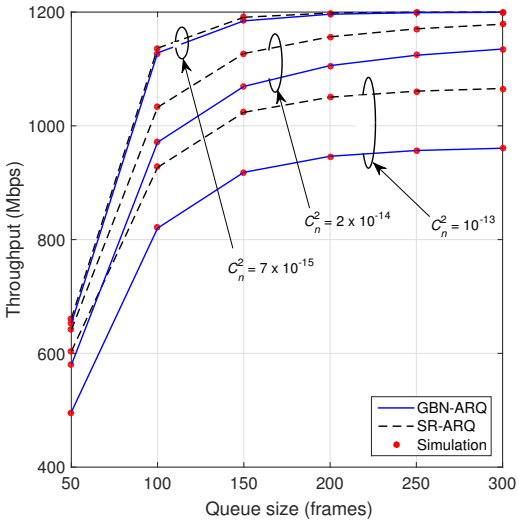

Figure 10: Throughput of GBN and SR-ARQ vs. queue size for different turbulence conditions.

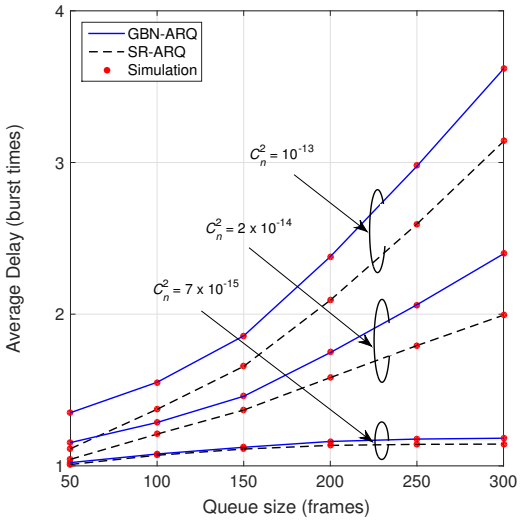

Figure 9: Average delay of GBN and SR-ARQ vs. queue size for different turbulence conditions.

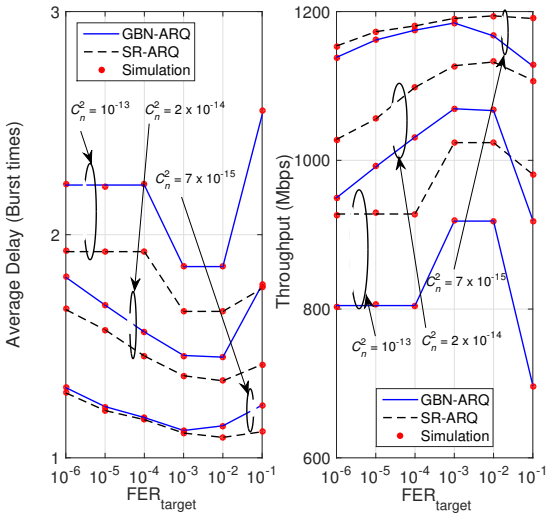

Figure 11: Average delay and throughput vs. target frame error rate for different turbulence conditions.

compared to the delay, which becomes very small thanks to high data rate. This leads to the inefficiency in throughput performance of SW-ARQ.

Next, we focus on the selection of the queue size for the operation of sliding window protocols. Figures 9 and 10 show the relationship between the obtained average delay and throughput versus the queue size when SNR = 25 dB, $\text{FER}_{\text{target}} = 10^{-3}$, and $\vartheta = 90$ (frames/burst time). We observe that when the queue size increases, the average delay increases. This is because the queue can accommodate more frames while still keep the erroneous ones for re-transmission at the head until they receive ACK signals from the receiver. This causes new arrivals to wait longer time in the queue. We also see the impact of turbulence conditions on the average delay. In the weak turbulence conditions, the average delay slowly increases and saturates while it significantly increases in the moderate-to-strong turbulence conditions. In addition to the average delay, the throughput also increases and reaches a certain level determined by rate of the highest possible transmission mode and the data traffic rate which enters the queue while the queue size keeps increasing. To select the queue size, the rule of thumb here is that we need to maximize the throughput while not increase the average delay, which is important because delay is ultimate QoS perceived by some of the data applications, in different turbulence conditions. For instance, we want to retain the average delay below 2 burst times (= 1.8 ms) while reaching a high level of throughput in different turbulence conditions, from weak to strong. Therefore, in this system setting, it is recommended to use the queue size of 150 frames to meet that requirement.

Another important issue in the design of the adaptive-rate systems is the selection of the transmission modes for channel states, which can bring the highest possible data rate while maintaining a target frame error rate $\text{FER}_{\text{target}}$. Figure 11

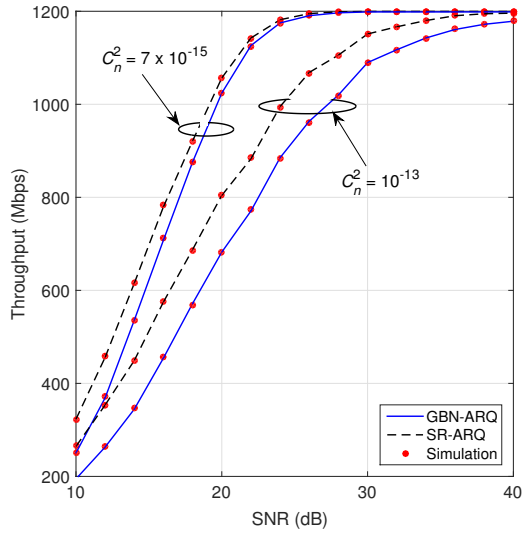

Figure 12: Throughput vs. SNR for different turbulence conditions.

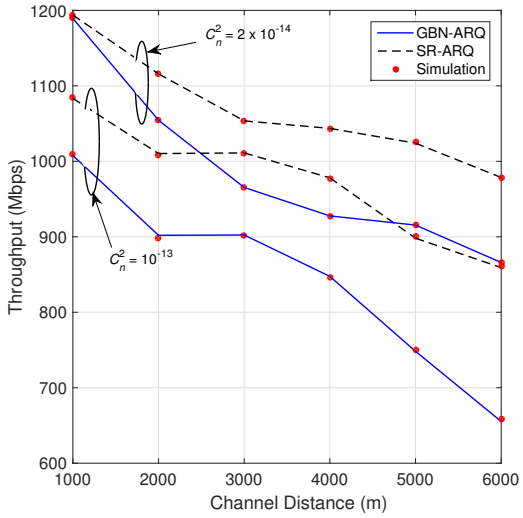

Figure 13: GBN and SR-ARQ throughput vs. channel distance.

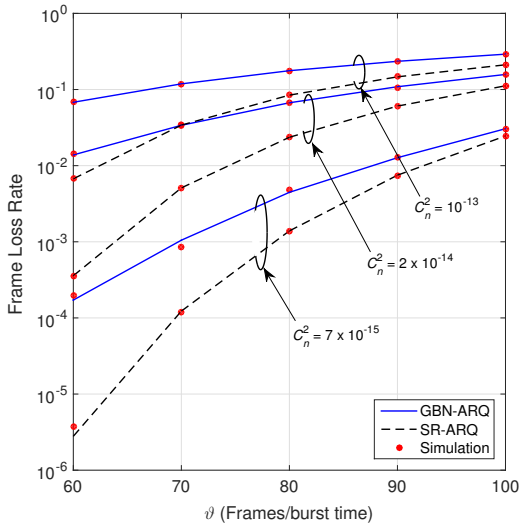

Figure 14: Frame loss rate vs. average arrival rates for different turbulence conditions.

investigates the effect of $\text{FER}_{\text{target}}$ on the average delay and throughput of both GBN-ARQ and SR-ARQ, when SNR = 25 dB, $\vartheta = 90$ (frames/burst time), and $Q = 150$ frames. Basically, for higher value of $\text{FER}_{\text{target}}$, the transmission rate increases but the FSO link becomes less reliable. In other words, we have more chances to choose higher transmission modes by choosing large $\text{FER}_{\text{target}}$. Nevertheless, the high probability of transmission errors may require many frame or burst retransmissions, which may increase the average delay and decrease the throughput performance. Therefore, there exists a value of $\text{FER}_{\text{target}}$ for which the average delay is minimized and throughput is maximized. From this figure, the optimal value of $\text{FER}_{\text{target}} = 10^{-3}$ is selected.

In Fig. 12, using $\text{FER}_{\text{target}} = 10^{-3}$ and queue size $Q = 150$ frames, we quantitively compare the throughput performance of GBN-ARQ and SR-ARQ in weak and strong turbulence conditions. As expected, SR-ARQ always provides a higher throughput than GBN-ARQ due to the fact that GBN-ARQ always discards all the frames in error burst even some of them are correct, while only erroneous frames are retransmitted in SR-ARQ. In addition, their throughputs are close in weak turbulence conditions, while SR-ARQ becomes clearly better than GBN-ARQ in the strong turbulence conditions.

Figure 13 investigates the possible transmission distances under the impact of turbulence, which gets stronger as the distance increases, given SNR = 25 dB, $\text{FER}_{\text{target}} = 10^{-3}\text{m}^{-2/3}$, $Q = 150$ frames, and $C_n^2 = 2\times10^{-14}$. Obviously, as the distance increases, the impact of turbulence degrades the throughput performance of both GBN and SR-ARQ protocols. The degradation of GBN-ARQ is more severe while the SR-ARQ performs much better than GBN-ARQ at a long distance. Using this result, one can decide the operation range of the designed system given a throughput requirement; for example, if 1 Gb/s connection is required even in the strong turbulence condition, the maximum distance is about 2 km when SR-ARQ is employed.

Figure 14 presents the frame loss rate versus average arrival rates for different turbulence conditions with SNR = 25 dB, $\text{FER}_{\text{target}} = 10^{-3}$, and $Q = 150$ frames. Evidently, stronger turbulence and/or higher arrival rate cause higher loss rate. Using this figure, one can set the limit on the data arrival accordingly to a QoS requirement in terms of the frame loss ratio for each ARQ protocols.

Finally, Fig. 15 illustrates the relation between the throughput performance versus the average received SNR (Fig. 15(a) and (b)) or queue size (Figs. 15(c) and (d)) over a range of average arrival rates. Also, $\text{FER}_{\text{target}} = 10^{-3}$ and $C_n^2 = 2\times10^{-14}$. In particular, using Figs. 15(a) and (b) with $Q = 150$ frames we, can find the minimum SNR required to reach a maximum throughput level at a certain average arrival rate. For example, when the average arrival rate is 60 frames/burst time, in order to reach the maximum throughput, the average SNRs required are 27 dB and 23 dB for GBN-ARQ and SR-ARQ, respectively. Similarly, using SNR = 25 dB in Figs. 15(c) and (d), we could design an optimal queue size to achieve

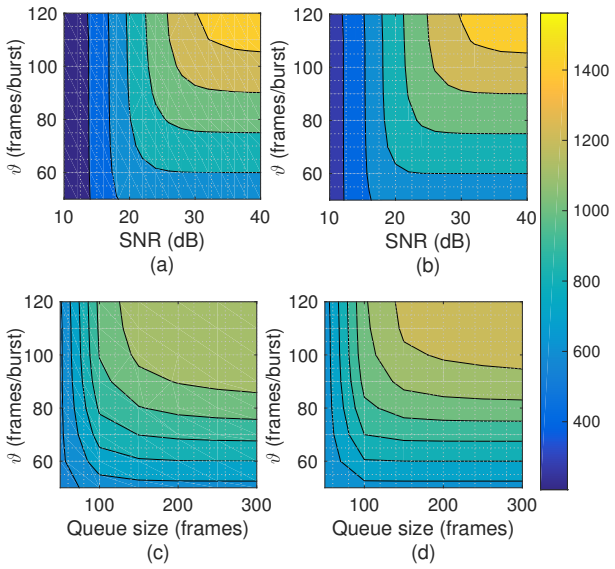

Figure 15: Throughput vs. average arrival rate with different average received SNR, given $Q = 150$ frames for (a) GBN-ARQ (b) SR-ARQ or with different queue size, given SNR = 25 dB for (c) GBN-ARQ (d) SR-ARQ.

a maximum throughput at a particular average arrival rate. For instance, the queue size should be designed to be 170 and 100 frames to guarantee the maximum throughput level when the average arrival rate of 60 frames/burst time for GBN-ARQ and SR-ARQ, respectively.

VI. Conclusion

We have proposed a design and queueing analytical framework for performance analysis of sliding window ARQ protocols with rate adaptation over FSO turbulence channels. To effectively facilitate the operation of sliding window protocols with AR transmission, burst-duration based window size was used. The time-varying behavior of the ΓΓ fading channels was modeled by a finite-state Markov model and the burst error model was developed. Another Markov model of the operation of protocols was also developed to analytically derive the system performance metrics of proposed design including frame loss rate, average delay, and throughput. Numerical results illustrated the impact of turbulence and supported the selection of optimal parameters, including the queue size, SNR, and the targeted FER. The theoretical analysis was also confirmed by Monte Carlo simulations.

References

[1] J. G. Andrews, S. Buzzi, W. Choi, S. V. Hanly, A. Lozano, A. C. K. Soong, and J. C. Zhang, "What will 5G be?," *IEEE Journal on Selected Areas in Communications*, vol. 32, pp. 1065–1082, June 2014.

[2] M. Jaber, M. A. Imran, R. Tafazolli, and A. Tukmanov, "5G backhaul challenges and emerging research directions: A survey," *IEEE Access*, vol. 4, pp. 1743–1766, 2016.

[3] B. Bag, A. Das, I. S. Ansari, A. ProkeÅ, C. Bose, and A. Chandra, "Performance analysis of hybrid FSO systems using FSO/RF-FSO link adaptation," *IEEE Photonics Journal*, vol. 10, pp. 1–17, June 2018.

[4] H. Kaushal and G. Kaddoum, "Optical communication in space: Challenges and mitigation techniques," *IEEE Communications Surveys Tutorials*, vol. 19, pp. 57–96, Firstquarter 2017.

[5] M. Safari, M. M. Rad, and M. Uysal, "Multi-hop relaying over the atmospheric poisson channel: Outage analysis and optimization," *IEEE Transactions on Communications*, vol. 60, pp. 817–829, March 2012.

[6] M. Safari and M. Uysal, "Relay-assisted free-space optical communication," *IEEE Transactions on Wireless Communications*, vol. 7, pp. 5441–5449, December 2008.

[7] E. Bayaki, R. Schober, and R. K. Mallik, "Performance analysis of MIMO free-space optical systems in Gamma-Gamma fading," *IEEE Transactions on Communications*, vol. 57, pp. 3415–3424, November 2009.

[8] I. B. Djordjevic, "Adaptive modulation and coding for free-space optical channels," *IEEE/OSA Journal of Optical Communications and Networking*, vol. 2, pp. 221–229, May 2010.

[9] A. García-Zambrana, C. Castillo-Vázquez, and B. Castillo-Vázquez, "Rate-adaptive FSO links over atmospheric turbulence channels by jointly using repetition coding and silence periods," *Optics Express*, vol. 18, pp. 25422–25440, November 2010.

[10] C. Abou-Rjeily and A. Slim, "Cooperative diversity for free-space optical communications: Transceiver design and performance analysis," *IEEE Transactions on Communications*, vol. 59, pp. 658–663, March 2011.

[11] M. Z. Hassan, M. J. Hossain, and J. Cheng, "Performance of non-adaptive and adaptive subcarrier intensity modulations in Gamma-Gamma turbulence," *IEEE Transactions on Communications*, vol. 61, pp. 2946–2957, July 2013.

[12] T. V. Pham, T. C. Thang, and A. T. Pham, "Average achievable rate of spatial diversity MIMO-FSO over correlated GammaGamma fading channels," *IEEE/OSA Journal of Optical Communications and Networking*, vol. 10, pp. 662–674, August 2018.

[13] K. Kiasaleh, "Hybrid ARQ for FSO communications through turbulent atmosphere," *IEEE Communications Letters*, vol. 14, pp. 866–868, September 2010.

[14] S. M. Aghajanzadeh and M. Uysal, "Information theoretic analysis of hybrid-arq protocols in coherent free-space optical systems," *IEEE Transactions on Communications*, vol. 60, pp. 1432–1442, May 2012.

[15] S. Parthasarathy, A. Kirstaedter, and D. Giggenbach, "Adaptive HARQ with channel state information in Inter-HAP FSO links," in *Photonic Networks; 18. ITG-Symposium*, pp. 1–6, May 2017.

[16] V. V. Mai and A. T. Pham, "Cross-layer designs and analysis of adaptive-rate transmission and ARQ for free-space optical communications," *IEEE Photonics Journal*, vol. 8, pp. 1–15, February 2016.

[17] A. Jurado-Navas, A. Garcia-Zambrana, and A. Puerta-Notario, "Efficient lognormal channel model for turbulent FSO communications," *Electronics Letters*, vol. 43, pp. 178–179, Feb 2007.

[18] A. Jurado-Navas, J. M. Garrido-Balsells, M. Castillo-Vázquez, and A. Puerta-Notario, "An efficient rate-adaptive transmission technique using shortened pulses for atmospheric optical communications," *Optics Express*, vol. 18, pp. 17346–17363, Aug 2010.

[19] H. D. Le, V. V. Mai, C. T. Nguyen, T. C. Thang, and A. T. Pham, "Modeling and throughput analysis of FSO systems using GBN-ARQ and AR transmission over atmospheric turbulence channels," in *2018 11th International Symposium on Communication Systems, Networks Digital Signal Processing (CSNDSP)*, pp. 1–6, July 2018.

[20] H. D. Le, V. V. Mai, C. T. Nguyen, and A. T. Pham, "Sliding window protocols with rate adaptation for FSO burst transmission over turbulence channels," in *2018 International Conference on Information and Communication Technology Convergence (ICTC)*, pp. 821–826, October 2018.

[21] C. Abou-Rjeily and W. Fawaz, "Buffer-aided relaying protocols for cooperative FSO communications," *IEEE Transactions on Wireless Communications*, vol. 16, pp. 8205–8219, Dec 2017.

[22] C. Abou-Rjeily and W. Fawaz, "Buffer-aided serial relaying for fso communications: Asymptotic analysis and impact of relay placement," *IEEE Transactions on Wireless Communications*, vol. 17, pp. 8299–8313, Dec 2018.

[23] L. B. Le, E. Hossain, and M. Zorzi, "Queueing analysis for GBN and SR ARQ protocols under dynamic radio link adaptation with non-zero feedback delay," *IEEE Transactions on Wireless Communications*, vol. 6, pp. 3418–3428, Sep. 2007.

[24] L. Badia, M. Rossi, and M. Zorzi, "SR ARQ packet delay statistics on Markov channels in the presence of variable arrival rate," *IEEE Transactions on Wireless Communications*, vol. 5, pp. 1639–1644, July 2006.

[25] G. Femenias, J. Ramis, and L. Carrasco, "Using two-dimensional Markov models and the effective-capacity approach for cross-layer design in AMC/ARQ-based wireless networks," *IEEE Transactions on Vehicular Technology*, vol. 58, pp. 4193–4203, Oct 2009.

[26] M. Z. Hassan, X. Song, and J. Cheng, "Subcarrier intensity modulated wireless optical communications with rectangular qam," *IEEE/OSA Journal of Optical Communications and Networking*, vol. 4, pp. 522–532, June 2012.

[27] B. T. Vu, N. T. Dang, T. C. Thang, and A. T. Pham, "Bit error rate analysis of rectangular QAM/FSO systems using an APD receiver over atmospheric turbulence channels," *IEEE/OSA Journal of Optical Communications and Networking*, vol. 5, pp. 437–446, May 2013.

[28] J. Yun and M. Kavehrad, "Markov error structure for throughput analysis of adaptive modulation systems combined with ARQ over correlated fading channels," *IEEE Transactions on Vehicular Technology*, vol. 54, pp. 235–245, January 2005.

[29] D. Giggenbach, W. Cowley, K. Grant, and N. Perlot, "Experimental verification of the limits of optical channel intensity reciprocity," *Applied Optics*, vol. 51, pp. 3145–3152, June 2012.

[30] R. L. P. Ammar Al-Habash, Larry C. Andrews, "Mathematical model for the irradiance probability density function of a laser beam propagating through turbulent media," *Optical Engineering*, vol. 40, pp. 40 – 40 – 9, 2001.

[31] H. T. Yura and S. G. Hanson, "Mean level signal crossing rate for an arbitrary stochastic process," *Journal of the Optical Society of American A*, vol. 27, pp. 797–807, April 2010.

[32] F. S. Vetelino, C. Young, and L. Andrews, "Fade statistics and aperture averaging for gaussian beam waves in moderate-to-strong turbulence," *Appied Optics*, vol. 46, pp. 3780–3789, June 2007.

[33] D. A. Luong, T. C. Thang, and A. T. Pham, "Effect of avalanche photodiode and thermal noises on the performance of binary phase-shift keying subcarrier-intensity modulation/free-space optical systems over turbulence channels," *IET Communications*, vol. 7, pp. 738–744, May 2013.

[34] A. Navas, J. M. Balsells, M. Vázquez, A. Notario, I. Monroy, and J. J. Olmos, "Fade statistics of m-turbulent optical links," *EURASIP Journal on Wireless Communications and Networking*, vol. 2017, no. 1, 2017.

[35] Z. Ji, I. Ganchev, and M. O'Droma, "Using a rayleigh fading channel and finite state markov model for analyzing the 'WBC over DVB-H' performance," in *2009 IEEE 70th Vehicular Technology Conference Fall*, pp. 1–4, September 2009.

[36] Q. Liu, S. Zhou, and G. B. Giannakis, "Cross-layer combining of adaptive modulation and coding with truncated ARQ over wireless links," *IEEE Transactions on Wireless Communications*, vol. 3, pp. 1746–1755, Sep. 2004.

[37] L. Kleinrock, *Theory, Volume 1, Queueing Systems*. New York, NY, USA: Wiley-Interscience, 1975.